A REVIEW OF ADDITIVE MANUFACTURING OF α- β TI ALLOY COMPONENTS THROUGH SELECTIVE LASER MELTING AND LASER METAL DEPOSITION

P. CHANDRAMOHAN[1,*], SHEPHERD BHERO[2],
K. MANIKANDASUBRAMANIAN[3], B. RAVISHANKAR[4]

[1]Department of Metallurgy, University of Johannesburg, South Africa 2028 and
Department of Mechanical Engineering, Sri Ramakrishna Engineering College, India
[2]Department of Metallurgy, University of Johannesburg, South Africa 2028
[3]Department of Mechanical Engineering, Coimbatore Institute of Engineering and
Technology, India
[4]Department of Metallurgical and Materials Engineering, National Institute of Technology,
Trichy, India
*Corresponding author-email: pcmohu@yahoo.co.in

Abstract

Additive Manufacturing (AM) is a rapid prototyping technique extensively used to build complex structures and intricate shapes without the necessity of post process machining. This process exists for two decades and still needs to attain its growth in order to meet the commercial requirements. In this article, Laser Metal Deposition (LMD) and Selective Laser Melting (SLM) of α-β titanium alloys and CP-Ti are reviewed. The reported investigations are categorized into 2 major classifications, namely:(i) Micro and macro structure and resulting mechanical properties of α-β Ti and CP-Ti, (ii) Effect of process parameters. Scholarly publications on SLM and LMD of α-β Ti alloys and CP-Ti are surveyed. The limitations of this emerging but promising method of manufacture are discussed.

Keywords: Laser, Additive manufacturing, Titanium alloys, SLM, LMD.

1. Introduction and Overview of Additive Manufacturing

Additive Manufacturing (AM) is a process that builds layer by layer by combining the technologies such as powder metallurgy, solidification, CAD-CAM and rapid prototyping [1-3]. Common AM technologies include Selective Laser Sintering (SLS), Laser Metal Deposition (LMD), Selective Laser Melting

Nomenclatures

[Al]eq	Aluminium equivalent
Ra	Roughness average, μm
Ti-6Al-4V	Titanium alloy with 6% Al and 4% Vanadium

Greek Symbols

α	Alpha phase
α′	Alpha prime / Martensite
β	Beta phase

Abbreviations

AISI	American Iron and Steel Institute
AM	Additive Manufacturing
CAD	Computer aided design
CAM	Computer aided manufacturing
CG	Columnar grain
CP-Ti	Commercially pure titanium
DLD	Direct laser deposition
EBM	Electron Beam Melting
EBSD	Electron backscattered diffraction
FOD	Focal Offset Distance
HAP	Hydroxyapatite
HIPing	Hot isostatic pressing
HT	Heat treated
HV	Vickers hardness
IR	Infra-red
LENS	Laser Engineering Net Shape
LMD	Laser Metal Deposition
OIM	Orientation imaging microscopy
SEM	Scanning electron microscopy
SLM	Selective Laser Melting
SLS	Selective Laser Sintering
UTS	Ultimate tensile strength
YS	Yield strength

(SLM), Electron Beam Melting (EBM), LENS-Laser Engineering Net Shape (LENS) etc. These processes make use of thermal energy to melt polymeric, metallic or ceramic materials before deposition and solidification into desired patterns. Lasers, electron beam, IR-light are typical energy sources available in additive manufacturing. Among these, laser is the predominantly used source and the schematic picture of LMD and SLM processes that make use of laser are shown in Fig. 1. In SLS, powders are partially melted while powders are fully melted in SLM and EBM processes [4-7].

In LMD or laser cladding, graded or pure metal in the form of wire or powder is melted and deposited layer by layer over a substrate to build components and it can also be used in repair work [8]. Large components can be better made by wire based laser techniques rather than powder based laser techniques due to its higher deposition rates of up to 0.7 kg/h [9]. Powder characteristics such as shape, size, distribution and processing parameters such as layer thickness, energy source,

energy intensity, scan/deposition speed, spot size and spacing distance are all important considerations in AM [10-12].
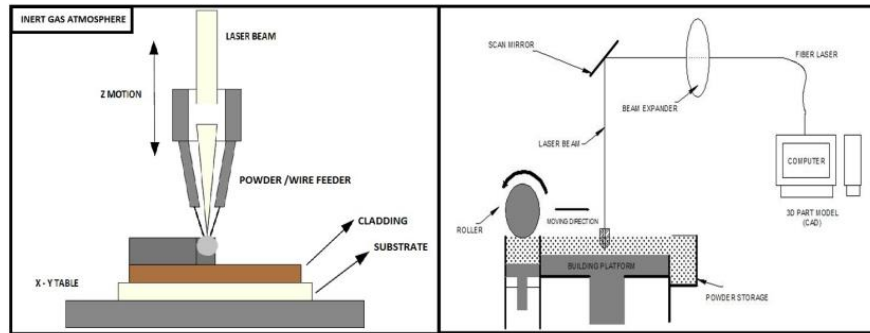

Fig. 1. Schematic picture of LMD and SLM.

The wavelength of laser determines the amount of energy released to the powder. In case of metal powders, laser absorption decreases as wavelength increases and vice versa. However, the reverse is true for ceramic and polymer powders. The laser wavelength should be selected specifically to suit a particular metal due to differences in absorption characteristics [13]. Nd:YAG lasers are suitable for metallic powders while CO_2 lasers are well-suited for polymeric powders [14, 15].

The core problem in AM lies in the poor fusion of successive layers, particularly in the case of ceramics. The problem is less pronounced in metals. SLM technique is applied for making components of different metallic materials such as AISI 316L austenitic stainless steel, hot-work steel, tool steel, maraging steel, CP-titanium, titanium-based alloys, Inconel, aluminium-based alloys, cobalt-based alloys, gold and copper [16]. Aerospace and medical industries are beginning to adopt these technologies. Recently, the availability of low-cost titanium powders in the market has encouraged cost-sensitive automotive industries to consider AM technologies [17].

Even though some advances have been made in AM, challenges still exist for users to gain full confidence in the viability of the technology. Homogeneity in the longitudinal and transverse direction has to be characterized to prove the integrity of components. Furthermore, the orientation of deposition should be determined in order to reduce the support structures which are not recyclable [18]. Simultaneously, establishment of Quality management framework in specific areas like product design and occupation hazard is very much required to make use of its technical developments in key areas like aerospace, medical field, etc. [19]. There are also some implications in the development of AM technology related to military ethics and security as the design can be easily copied via the CAD-CAM file, re-engineer from the category of small arms (Guns) to major military hardware [20].

Some previous studies and reviews reported that direct laser deposition (DLD) process can be employed in fabricating metallic parts [21]. In some cases, AM technologies have been used for multiple materials that include plastic polymers, metal materials and ceramic materials [22, 23]. Additive manufacturing of

metallic material includes qualification of materials, processing models and use of sensors and controls [24]. A report on various AM technologies and equipment manufacturers have been published [25]. There has been no specific publication on SLM and LMD of the various α-β Ti alloys and CP-Ti in the literature. Hence the focus is made on the present review article with following objectives:

- Determine the range of Ti alloy components that can be produced by additive manufacturing.
- Characterize the structure and study of mechanical properties by selective laser manufacturing of Ti-6Al-4V in as-formed and in heat treated condition in comparison with its wrought and EBM equivalents.
- Evaluate the mechanical properties of laser formed CP-Ti and α/β Ti alloys.
- Assess the response of process parameters on SLM/LMD formed Ti-6Al-4V, Ti-6Al-4V composite, CP-Ti and other α-β Ti alloys.

2. Literature Review

2.1. Additive manufacturing of Ti-6Al-4V: Structure and mechanical properties:

An overview of the metallographic investigations on the as-formed Ti-6Al-4V from selective laser melting and laser metal deposition as well as in their heat treated condition is presented in this section. Also the resulting mechanical properties are discussed. A summary of the process and outcome are consolidated and presented in Table 1.

Table 1. Structure and properties of SLM/LMD as-formed and HT Ti-6Al-4V.

Process	Outcome	Reference
SLM-As cast, HT, Vibration, Laser surface texturing	Microstructure, hardness, UTS and ductility	26, 27, 30, 31, 33, 37, 38, 39, 40, 41, 42.
LMD-As deposited, HT, Control system	Microstructure, Strain and fatigue	9, 28, 29, 34, 35, 36
SLM/LMD Vs Wrought	Surface finish, microstructure UTS,YS, ductility and creep rate	43, 44, 45, 46, 47

Standard microstructures of Ti-6Al-4V formed by SLM processes at different conditions are shown in Fig. 2. The optical microscopy of as-sintered SLM made horizontal built and vertical built structures reveal fine martensitic phase which gets converted into α+β upon heat treatment at higher temperatures. From the SEM picture of the as-sintered specimen, the average grain width is measured around 4 μm. Grain growth from 4.03 to 9.42 μm is noticed after HT 1, since the specimen temperature were elevated above β transus and slow cooled. In HT 2, where the specimens were heated below β transus and air cooled, grain refinement were observed with an average width ranging from 2.03 to 3.89 μm. [26].

The microstructural evolution with thermal treatment is invariably accompanied by changes in mechanical properties. Therefore, engineering applications of Ti-6Al-4V alloy at higher temperatures need to consider these

phase transformations as well as the selection of temperature regimes that bring about desired mechanical properties.
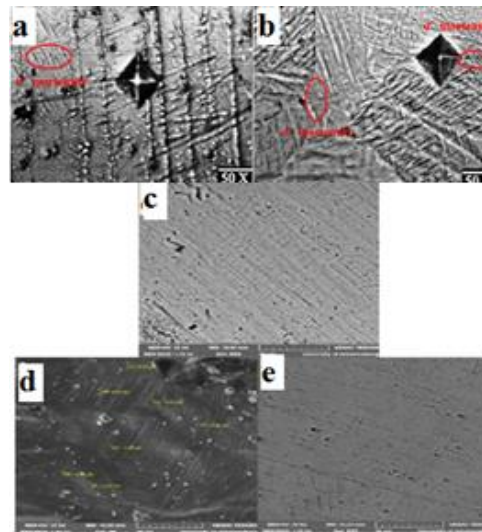

Fig. 2. Microstructures of SLM made Ti-6Al-4V parts (a) as-sintered horizontal built up (b) as-sintered vertical built up (c) SEM analysis of as-sintered (d) SEM analysis of above β transus and slow cooled and (e) SEM analysis of below β transus and air cooled [26].

The microstructural evaluation of SLM processed Ti-6Al-4V alloy reveals the presence of ά-martensite phase and grains become elongated due to the occurrence of epitaxial growth. Precipitation of intermetallic phase Ti$_3$Al is also noticed at high heat inputs during the deposition process [27]. Without post heat treatment, a unique combination of high UTS (1060 MPa) and improved ductility (14% elongation) has been achieved in a Ti-6Al-4V direct energy deposited 3D cruciform component, which is attributed to the integrity compact devoid of pores, low concentration of oxygen (0.0124 wt.%) and reduced α-lath width due to different cooling rate at varying heights [28]. Abdalla et al. [29] devised a closed loop control system to build Ti-6Al-4V at a temperature below 415°C to achieve better alignment of prior-β grains. In addition, α-lath became more uniform with less diffusion of alloying elements within the compact. Hence a uniform microhardness values was achieved. Wei-Chin et al. [30] used electromagnetic vibrations in SLM process to control the cooling rate of Ti-6Al-4V alloy during solidification. Grain refinement was attributed to the magnetic flux however, mechanism was not fully explained. Xu et al. [31] predicted the determining parameters to achieve ultrafine lamellar structure of α+β by way of ά martensite decomposition in the SLM-fabricated Ti-6Al-4V. These included a power rating of 375 W, laser scanning velocity of 1029 mm/s, layer thickness of 60 μm and Focal Offset Distance (FOD) of 2 mm.

Few post heat treatment studies have been carried out at different temperatures in the recent period on laser formed Ti-6Al-4V. The resulting microstructure and mechanical properties are further explained. The decomposition of ά martensite was reported to take place at temperatures at a lower level of 400°C during post-SLM

heat treatment resulting in high yield strength of greater than 1100 MPa and 11.4% elongation [31]. In a similar work, Russell et al. [32] reported that hexagonal ά martensite causes only limited hardening effect due to high dislocation density and fine lamellar structure. Furthermore, temperature distribution during the laser melting of Ti-6Al-4V alloy and increased holding time in post heat treatment up to 960°C lead to the formation of uniform distribution of globular α phase, which is desirable for implant materials [33].

Erhard et al. [34, 35] recommended post heat treatment to homogenize the microstructure of Ti-6Al-4V thereby avoiding scattering in mechanical properties. Conversely, the post heat treatment at 600 °C for 4 h did not change the morphology and microstructure. Soaking at 1200°C for 2 h reduce the average hardness from 327 to 311 HV with destabilization of the as-built macrostructure. In a similar work, by heat treating above β transus temperature, the change of columnar to globular β-grains was made possible. Cooling rate from above β transus influences the microstructure and hardness more than the holding temperatures above β transus [36]. In contrary, a recent research on heat treatment from 300 to 1020°C reports that at or below 600°C the as-received acicular morphology partially decomposes into platelet. Maximum hardness is recorded for the treated temperature of 500° C which is due to the partial decomposition of martensite into in-situ transitional substructures and its refinement [37].

Bernd et al. [9] studied the microstructure and grain orientation of Ti-6Al-4V formed from wire-based additive laser melting technique. It was reported that prior β-grains were elongated and surfaces were layered with banded meso-structures. Furthermore, there was presence of fine lamellar α/β structures at the top field of laser beam component than the bottom field which yielded high ultimate tensile strength (UTS). Grain orientation is a fundamental consideration in the design and forming of aerospace components. Preferential orientation in z-direction favours ductility on the top region. Thus, to have uniform properties along the component, about 10 mm layer should be removed. The heat treatment at 600 °C for 4 h does not influence significantly on the mechanical properties. However, heat treatment at 843°C increases considerably the strain to failure. After heat treatment at 680 °C for 4h, ά martensite transformed to a mixture of α and β, with α phase having a width in between 500 and 800 nm. The microhardness decreased from 408±35 HV to 378±35 HV, which was attributed to the coarsening of the microstructure [38]. Vrancken et al. [39] conducted a study on effect of 10 wt% Mo in Ti-6Al-4V-ELI processed by SLM. After heat treatment at 650°C extremely fine two-phase α+β microstructure was observed. The mechanical properties showed a higher hardness of 468±7 HV against a hardness of 399 HV for as-built part. After heat treatment at 900°C and 1050°C the resulting microstructure was fully β, leading to the inference that β transus temperature was reduced to about 900 °C.

The evaluation of under laser surface texturing (Linear-45%, Dimple-20% geometry) with a microstructure of α, 5 - 10% β grains and few TiO_2 showed an improvement on the nano-hardness from 203 HV to 611 HV. Texturing also reduced the wear rate due to improvement in micro-hardness and grain refinement which is due to the formation of oxide phases on the textured zone [40, 41]. Recent research about the level of orientation in SLM made sample reports preferred orientation in the microstructure but not inside its ingredient powder. Also it is stated that the orientation of its bulk cell is preferred towards the hexagonal basal plane [42].

2.1.1. Additive manufacturing SLM/LMD versus Wrought Ti-6Al-4V

This subsection compares the performance of Ti-6Al-4V components manufactured by SLM and LMD against wrought Ti-6Al-4V with respect to the metallographic and surface finish. The resulting mechanical properties are summarized in Table 1.

Alcisto et al. [43] compared the laser-formed Ti-6Al-4V materials with that of conventional wrought alloy equivalent and found that the laser formed samples had comparable tensile strength with reduced elongation but inferior surface finish. The yield strength of 964 MPa and UTS of 1041 MPa were found to be higher in the SLM samples than the wrought samples that gave a yield strength of 948 MPa and UTS of 994 MPa which is due to the difference in preferred orientation resulting from epitaxial growth of layer by layer build up and rolling respectively. Percentage elongation was lower for SLM rod than the wrought product. In the transverse direction, samples of SLM had higher YS (1058 MPa) and UTS (1114 MPa) than in the longitudinal direction. In other words, transverse elongation is 5% while longitudinal elongation is 7% [44]. Alcisto et al. [43] further studied the effect of position where a tensile specimen is sectioned from the laser as-deposited plate. They reported anisotropy in the tensile values showing higher tensile values in *x* and lower in *z* direction. In the machined and heat treated laser formed plates, the tensile properties remained isotropic within the plane. Acicular α-β was observed with high porosity in columnar β grains in the as-deposited while the heat treated had minimum porosity in coarse Widmanstätten α grains.

Myriam et al. [45] used quasi-continuous pulsed mode laser in the metallic deposition of Ti-6Al-4V and reported an improved surface finish with little post-machining steps, when compared with the fully continuous wave heating. At times, aiming to improve the surface finish is also detrimental in application point of view. A recent research on improving surface finish by selective remelting of surface layer reports that corrosion resistance and biocompatibility gets reduced due to the higher concentration of aluminium and vanadium on the surface [46]. The Widmanstatten structure in the Ti-6Al-4V alloy was reported to be more resistant to oxidation than the equi-axed. Short-term creep tests showed that the equi-axed microstructure possess twice the creep rate as that of Widmanstatten structure. The higher creep resistance of the Widmanstatten microstructure is due to the obstruction created by α-β interfaces to the motion of dislocation, average grain size (395 μm), reducing the sliding of grain boundaries, dislocation sources and oxygen diffusion in grain boundaries [47].

2.1.2. SLM/LMD versus EBM in Ti-6Al-4V

A comparison between SLM/LMD and EBM of Ti-6Al-4V is discussed in this subsection.

Haijun et al. [48] compared Ti-6Al-4V alloy fabricated through SLM and EBM processes with respect to structure, mechanical properties, porosity and surface finish. The Yield Strength and Ultimate Tensile Strength of SLM were found to be higher than those of EBM samples as a result of α' martensite structure. However, fatigue strength and hardness of the samples of both SLM and EBM are comparable. The microstructure is largely determined by the rate of cooling in both

processes. Upto 1 vol. % porosity, the properties such as tensile, fatigue strength and hardness are not changed as much in SLM samples. The porosity of 5 vol.% has considerable detrimental effect on the mechanical properties. A recent research aimed at relating porosity with fatigue life also recommends for less than 1% porosity to achieve better fatigue life [49].

In a related work it was reported that SLM-made samples yield better surface finish than that of EBM-made samples [50]. In a recent research finding on the effect of porosity and microstructure of EBM made part, porosity is said to be the primary deciding factor of its mechanical properties [51]. Haijun et al. [52] compared SLM with EBM in susceptibility to defect formation on Ti-6Al-4V during additive manufacturing. It is reported that the high energy density in SLM causes over-melting of powder bed and the defects result from vaporization within the melt pool. Conversely, the EBM system uses a more complicated feedback control design which prevents formation of these types of defects. In SLM, defects such as pits are produced on the surface which is not observed in the EBM system. Discontinuities in melt pool and absence of melt pool overlap results in defects, however, laser deposition has better UTS and YS than EBM and wrought grades. Anisotropy behaviour is not noted much in the mechanical property of the laser deposited Ti-6Al-4V alloy in spite of the prior-β columnar grains that grew epitaxially along the deposition direction [53].

Recent research findings of Tiferet et al. [42] revealed that strain free components can be produced in EBM without post heat treatment where it is not so with SLM. Gary and Eric [1] compared laser metal deposition, LENS and direct laser fabrication (DLF) to fabricate Ti-6Al-4V alloy. It is reported that single step processing of DLF yields the tensile yield strength comparable to that of wrought material with an elongation of 6%, which is lower than 10% for wrought specimens. A complete melt is achieved by mixing 80% Ti and 20% Nb powders at the laser focal zone and increasing laser power from 200 W to 320 W. In general, combining these two processes in single step gave deposition accuracy within 0.12 mm and surface finish of 10 μm. Feeding powders separately during printing is better to avoid segregation of blended powders based on powder density, size, shape, and surface characteristics during agitation by feed systems.

2.2. Laser deposition of other-α/β Ti alloys and CP-Ti: Microstructure and properties

The summary of laser deposited α/β Ti alloys and CP-Ti are listed in Table 2. The as-deposited Ti-6.5Al-3.5Mo-1.5Zr-0.3Si sample shows unique grain morphology of both columnar and equi-axed grains with the presence of intra-granular basket-weave type microstructure. A bimodal microstructure of α lath (crab-like) and Widmanstätten α colony with transformed β was observed in α+β annealed condition and under β annealing treatment approximately above 900 ºC, transformation occurs from columnar to equi-axed grain morphology thereby reducing tensile anisotropy [54, 55]. The macrostructure comprises two zones; the unstable one (3 - 4 mm) at the top region and stable one at the bottom region. The stable and unstable zones had a microhardness value of 375 HV and 363 HV respectively. The higher hardness of stable zone is due to α phase fraction in high volumes and higher solid solubility (Al diffusion into α-phase) [56].

Tensile strengths and elongation of laser deposited samples are poor when compared to that of wrought equivalents as a result of larger grains and their perpendicular orientation to the direction of loading [50]. However, Yanyan et al. [56] reported that the strength and elongation of the same alloy increase with increasing size of prior-β-grain which is due to the severe strain caused by mismatch between prior-β-grains rather than resistance to dislocation motion [57]. The grain morphology of the same alloy on the substrate of hot-rolled CP-Ti plate reveal fine equi-axed grains in the sub-surface zone and large basket-weave grains in the lowest region. Deposition rate also determines the grain morphology. Low rate of mass deposition could lead to production of full columnar grains and high mass deposition rate produces equi-axed grains [58].

Table 2. Structure and properties of laser deposited α/β Ti alloys and CP-Ti.

Process	Outcome	Reference
LMD-Ti-6.5Al-3.5Mo-1.5Zr-0.3Si	Micro/macro	54, 55, 56, 57, 58,
LMD-Ti-6Al-2Zr-1Mo-1V	structure,	59, 60, 61, 62, 63,
LMD-Ti-5Al-5Mo-5V-1Cr-1Fe	microhardness,	64, 65, 66, 67, 68
LMD-Ti-5Al-5Mo-5V-1Cr-1Fe- HT	UTS, ductility,	
LMD-Ti60A- HT	Young's	
LMD-TC21	modulus, elastic	
CP-Ti and	modulus,	
Ti-6Al-2Zr-1Mo-1V	plasticity,	
Ti-4Al-1.5Mn-HT	compressive,	
CP-Ti and Ti-TiB composites-	grainmorphology,	
Porosity effect	texture	

A common structural Ti-alloy (Ti-6Al-2Zr-1Mo-1V) containing maximum amount of α-phase and minimum amount of β-phase along with a low alloy, low-cost α Ti-alloy (Grade 2 CP-Ti) were laser deposited on a substrate alternately to form a structurally graded material. The microstructure of the subsequent deposition reveals equi-axed grains with Widmanstatten α-laths and the early deposition reveals large columnar grains with fine basket-weave structure. Increase in [Al]eq was accompanied by an increase in hardness as a result of solid solution and grain boundary strengthening [59, 60].

In a similar work, the laser melt deposition technique was used to fabricate Ti-5Al-5Mo-5V-1Cr-1Fe alloy. The microstructure revealed bamboo-like β grain morphology at macro level with fine basket-weave structure and α grain boundary. Due to the fine microstructure, the as-deposited samples yield high UTS of about 1178 MPa and a lower elongation of about 5% only. High UTS is due to rapid cooling and the dispersion strengthening effects. Low ductility is due to the inter-granular continuous α phase [61]. When subjected to sub-transus annealing treatment at 860° C for 4 h, the aspect ratio of α phase did not decrease due to the progressive globularization of α plate by diffusion process. However, the sub-transus treatment at 860º C for 1 h, decreases the aspect ratio of α phase to 1.7 with near equi-axed morphology [62].

Laser deposited Ti-60Al (Ti-5.54Al-3.38Sn-3.34Zr-0.37Mo-0.46Si) alloy was subjected to cyclic thermal exposure tests at 800° C (50, 250, 500 and 750° C) for 120 s followed by compressed air cooling to 150° C in 60 s. It is reported that the β phase transforms from its fine basket-weave shape to wedge-like and then

finally to a granular shape. The α-phase which was initially around 78.5% increased to 97.6% and coarsened with thermal exposure cycles. Micro-hardness values showed a linear increase with temperature and the maximum hardness was 33.3% more than the as-deposited sample subjected to 750° C. Solid-solution strengthening effect of oxygen dissolution during cyclic thermal exposure lead to the increase in hardness [63].

Qiang et al. [64] characterized the microstructure of Ti alloy, TC21 (Ti-6Al-2Zr-2Sn-3Mo-1.5Cr-2Nb). Microstructural analysis revealed rib-like α phase at the bottom and acicular martensite α′ at the top of the sample. The same alloy characterized by Zhuo Li et al. reports fine basket-weave microstructure of α laths with meta stable β phase [65].

Further investigation on the comparative mechanical behaviour of CP-Ti and Ti-6Al-2Zr-1Mo-1V structurally graded materials (SGMs) produced by LAM show that the strength of all SGM tensile specimens are higher than those of the monolithic CP-Ti specimens, except the SGM specimen of 10 mm gauge diameter. Thus, the SGM showed potential for use as load-bearing-components due to its good strength-ductility balance [66].

Ti-4Al-1.5Mn alloy was laser deposited and it was reported that the α+β phase region at different temperatures resulted in a bi-modal microstructure including α′, which looks like crab claw and β transformed to fine lamellar. Annealing the alloy at 955° C resulted in 35% of crab-claw-like α′ that facilitates maximum impact toughness. Bi-modal microstructure leads to a good combination of strength and ductility under impact load as it acts as obstacles for crack propagation [67].

Microstructural investigations on Ti-TiB and CP-Ti composites with different porosity levels of 10%, 17% and 37% indicated an alpha prime martensitic (α′) and needle-like shape morphology of particles of TiB distributed in α-Ti matrix. With increase in porosity, the Young's modulus and compressive strengths decreased. Young's modulus decreased sharply from 113 GPa to 13 GPa and 145 to 25 GPa for CP-Ti and Ti-TiB respectively [68].

2.3. Effect of laser process parameters

An overview on the effect of process parameters such as laser scanning speed, Laser power, gas flow rate, powder flow rate, etc., on SLM/LMD processed T64, Ti-6Al-4V composites, CP-Ti and other α-β Ti alloys are discussed in this section.

2.3.1. SLM/LMD made Ti-6Al-4V

The summary of findings on the effect of process parameters on Ti-6Al-4V formed by SLM/LMD is given in Table 3.

The initial process parameters optimization were carried out to minimize porosity in the SLM processed Ti-6Al-4V parts. Hot-isostatic pressing (HIPing) was also carried out to minimize internal stresses. With increase in scanning velocity of laser beam, the number of pores increase and a larger spot size is recommended to reduce porosity. Heat treatment does not improve ductility in SLM processed material whereas with HIP, ductility increase up to 19.4% due to the transformation of martensite to lamellar α+β phases. Hence HIP is

recommended for cyclically loaded components [26, 69]. Similarly in another work, it is also reported that HIPing of Ti-6Al-4V components reduce the porosity from 3.05% to 0.81% due to the presence of homogenous α+β microstructure [70]. In order to obtain isotropic stress field in SLM made component, it is recommended to maintain short scan vector lengths and uniform orientation of scan vectors [71].

Rasheedat et al. [72] reported that change in laser power during the deposition of Ti-6Al-4V powder on Ti-6Al-4V resulted in the formation of layer band even in single layer deposition which was attributed to shrinkage during solidification in the fusion zone. With increase in laser power, the density of columnar β grain decrease and the microstructure of the heat affected zone (HAZ) consisted of fine and coarse globular α′ . The microstructure also revealed fine to thick martensite with an increase in the average micro hardness values. In another work, the experimental design and analysis using the Design Expert 9 revealed that micro-hardness was inversely proportional to the laser power, while scanning speed was found to be directly proportional to the micro hardness of Ti-6Al-4V powder deposited on T64 [73].

Table. 3. Effect of process parameters on SLM/LMD.

Process	Outcome	Reference
Ti-6Al-4V		
SLM-Ti64-HIP-Scan velocity	Porosity	26, 71-77, 80, 81
LMD-Ti64-Laser power, Design and analysis on laser power, welding speed, wire feed rate, Cooling rate and section size, Building time, strategy and incident energy	Microstructure, micro hardness UTS and YS	8, 34
Ti-6Al-4V alloy composite		
LMD-Ti64/TiC composite-Laser power, scan velocity, Powder flow rate	Microstructure, micro hardness and wear.	78-81
LMD-Ti64 wire and TiC-powder flow rate.	Microstructure, hardness wear, UTS, ductility, compressive strength, bonding, fracture toughness and elastic properties	
LMD-Ti64 wire and WC-Powder flow rate		
Laser surface nitriding- Ti64 -Gas flow rate		78-81
HAP Coating deposition-Laser power		
CP-Ti and other α-β		
SLM-CP-Ti, SLM-CP-Ti and Ti-TiB, SLM-Ti-24Nb-4Zr-8Sn Laser power, scan speed, linear energy density	Microstructure, micro hardness, UTS and compressive strength, wear, molten pool life time, width and temperature, density and young's modulus	86-89, 91
LMD-Ti-5Al-5Mo-5V-3Cr-Laser power, scan speed and powder flow rate	Microstructure and build height	90

Single and multi-bead laser deposition studies were conducted on Ti-6Al-4V substrate using Ti-6Al-4V wire containing ultra-low interstitial atoms by changing the parameters of laser power, wire-feed and welding speed. The microstructure varies from globular α-grains in a basket-weave (α+β) matrix to columnar β-grains comprising of basket-weave (α+β) at different zones. Increase in wire-feed speed and laser beam power led to grain coarsening in the melted zone or columnar grain (CG) zone and heat affected zone. Hardness depends on the process parameters in both zones. The hardness of solidified melt pool (CG zone) in single bead deposition increased with the amount of base material in the melt pool due to the presence of higher amount of interstitial impurities such as O, C and N. In multi-bead deposition, the contamination from the base material becomes negligible after a few initial layers. Hence the hardness values of multi-bead were different from those of single bead deposition [74, 75].

Similarly, Tarak et al. [76] reported the effect of cooling rate on the mechanical properties and microstructure of laser deposited Ti-6Al-4V step shaped samples. The microstructure reveals fine α′ with increase in the aspect ratio due to the faster rate of cooling. Increasing the cooling rate and reducing the substrate size, increases the YS, UTS and hardness remarkably. The increase in strength was due to the formation of fine needle-like α-phase from coarse plate-like α. In a related work, the effects of building technique and incident energy on laser cladding of Ti-6Al-4V reveal that the building time was more dependent on clad thickness than the building technique. Cladded material shows higher UTS with better ductility than the substrate [8]. In a recent study made on the influence of scan speed for scan spacing in SLM of Ti-6Al-4Valloy, higher valued scan spacing (600 mm/s) results in finer structure with higher α′ martensite needles and lower valued scan spacing (300 mm/s) results in more acicular martensite [77]. Erhard et al. [34] deposited blocks using a Nd:YAG laser on Ti-6Al-4V wire with two sets of parameters (laser power of 2.625 and 3.5 kW; deposition speed, 10,7.5 mm/s; wire feed speed, 30, 40 mm/s) followed by post heat treatment at different conditions (as-built, 600° C for 4 h and 1200° C for 2h). Post heat treatment has major effect on the hardness of the blocks than the process parameters.

2.3.2. LMD made Ti-6Al-4V alloy composite

The studies reported on effect of process parameters on LMD made Ti-6Al-4V alloy composite are summarized and presented in Table 3.

Rasheedat et al. [78, 79] investigated the influence of scanning velocity and laser power on the microstructure, microhardness, and wear resistant property of laser deposited 50% Ti-6Al-4V/50% TiC composite. It is reported that the optimal laser power and scanning velocity for better wear resistance performance are 2 kW and 0.065 m/s respectively. Microstructure reveals a moderate density of small size unmelted carbides that act as lubricant to improve the sliding wear property despite a slightly higher roughness value (Ra) of 0.911 μm. Furthermore, with respect to the powder flow rate, least wear volume of 0.000024 mm^3 was found to occur at a laser power of 3 kW and with powder flow rate of 2 g/min for a scanning speed of 0.05 m/s. Formation of Ti_3Al at such high power also contributes for the powder formation that favours smooth sliding [80]. In case of the multi-layer (4 numbers) deposition made in the same material, the optimized process parameters of laser power 2.07 kW, scanning speed 0.00083 m/s, powder

flow rate 2 rpm and gas flow rate 2 l/min yield taller (5229.51 µm) deposit than the one (4983.51 µm) made using constant process parameters of laser power 2.5 kW, scanning speed 0.01 m/s, powder flow rate 2 rpm and gas flow rate 2 l/min. The microstructure reveals the presence of α-Ti, TiC (49%), intermetallic compound Ti_3Al (22%). The sample produced with the optimized-process parameters had higher micro hardness of 1200 VHN with lowest wear volume of 0.021 mm^3 against 0.12 and 0.033 mm3 for the substrate and constant process parameters respectively [81].

A study on flow rate of TiC powder in the order of 0.14, 0.3, 0.44, 0.57, 0.7, 0.87, 1.03 g/min during laser deposition using Ti-6Al-4V wire on rolled Ti-6Al-4V substrate followed by HIPing at 103 MPa pressure and 930 ºC for 4 h, reveal that uniform spread of TiC in all the samples improve the sliding wear resistance at its volume fraction more than 24%, but compromising the ductility [82]. In an another work by Farayibi et al. [83], tungsten carbide powder feed rates of 10 to 40 g/min during the simultaneous laser deposition with Ti-6Al-4V wire on Ti-6Al-4V substrate produce a microstructure with W, C, TiC, and β-TiC. If the powder feed rate is increased, mean hardness values also increases in the range of 600 to1030 HV due to the two-phase precipitation of W and TiC at the clad centre and WC particles at its periphery. Jyotsna [84] studied the effect of laser parameters on the characteristics of the Ti-6Al-4V surface nitrided layer from 300 to1100 µm. The microstructure consisted of dispersed TiN in α-Ti matrix. This resulted in increased micro hardness from 280 VHN (untreated) to 600-1200 VHN. As the gas flow rate is increased from 5 l/min to 10 l/min, the residual stress developed in the surface varied from 250 MPa to 750 MPa for the applied power of 600 W to 700 W. The compressive strength increased from 1400 MPa to 2500 MPa at a power of 800 W. A related study on the effect of laser power while depositing hydroxyapatite (HAP) coatings on Ti-6Al-4V by melting at 750 W and 1.0 kW revealed that 750 W power facilitated nil dilution and achieved good microstructure, hardness of 678.5 HV at the interface and 165.9 HV on coating surface with a strong bonding of HAP with the substrate. The low hardness on the coated surface and high hardness at the interface probably indicated better fracture toughness and elastic properties [85].

2.3.3. SLM/LMD made CP-Ti and other α-β Ti alloys

The effect of process parameters like laser power, scan velocity, flow rate of gas and powder on SLM/LMD made CP-Ti and other α-β Ti alloys are reviewed in this section and the details are summarized in Table 3.

Attar et al. [86] processed CP-Ti parts using laser power-100W with scanning speeds above and below 100 mm/s without any post-treatment. Microstructure revealed fine α′ in the above 100 mm/s speeds and coarse plate like α′ grains in the below 100 mm/s speeds. Fine α′ formed from β, led to overall improvement in the micro-hardness (261 HV), compressive (1136 MPa) and tensile strengths (757 MPa), which is attributed to the increase in thermal and kinetics under-cooling. Similarly, in the SLM processed CP-Ti powder, for the scan speeds from 100 to 400 mm/s, the microstructure changed from relatively coarse lath-shaped α to refined acicular-shaped α′ and then further refined to zig-zag-structured α′. The scan speeds of 200 and 300 mm/s, linear energy density of 450 and 300 J/m yield the maximum densification of 99.5%. The other two combinations of low velocity

100 mm/s with high LED 900 J/m and high velocity 400 mm/s with low LED 225 J/m result in lower rate of densification due to the microscopic balling phenomenon, interlayer thermal cracks and presence of Marangoni convection which has caused liquid instability. The maximum hardness of 3.89 GPa, reduced coefficient of friction (CoF) of 0.98 and wear rate of 8.43×10^{-4} mm^3 N^{-1}m^{-1} were achieved using 300 mm/s and 300 J/ m. Improvement in the wear performance was attributed to the formation of tribo-layer, adhering plastically on the wear scar [87].

In another work, while processing CP-Ti by SLM with a laser scan speed of 100 mm/s and laser power of 150 W, Yali and Dongdong [88] achieved the maximum molten pool temperature as 2248 ºC and lifetime of liquid as 1.47 ms. By increasing the speed of scan from 50 to 200 mm/s, the molten pool width decrease from 137.1 to 93.8 µm and the depth from 64.2 to 38.5 µm. However, a power increase from 100 to 200 W increased the width from 71.2 to 141.4 µm and depth from 32.7 to 67.3 µm. Hooyar et al. [89] optimised the scan speed and laser power for the solid CP-Ti and Ti-TiB composites. Microstructural investigations revealed α-Ti matrix with TiB particles in needle shape as a result of chemical reaction of irregular-shape TiB$_2$ particles with pure Ti. Due to the grain refinement and hardening effects of TiB particles, micro-hardness and compressive strength improved remarkably at an optimum laser power of 185 W and scanning speed of 120 J.mm-3 without metal evaporation and key-hole effects.

An assessment made on the α-β Ti alloy (Ti-5Al-5Mo-5V-3Cr) on build geometry show that at higher laser power, the build height mainly depend on the powder flow rate and scanning speed. Additional increase in laser power by keeping the powder flow rate and scanning speed as constant, has little effect on build height, but coarsened the microstructure. As-fabricated samples were dominated by β grains. In situ dwelling and annealing promoted α-precipitation, which led to improved micro hardness closer to that of forged Ti5553.[90] Zhang et al. [91] also studied the effect of process parameters using increased scan speed of 550, 650 and 800 mm/s. The density and microhardness of Ti-24Nb-4Zr-8Sn alloy specimens decrease with increase in scan speed. A lower Young's modulus of 53 GPa and UTS of 665 MPa with not less than 10% ductility were reported for all the samples. The drop in elastic behaviour was attributed to the 0.21 wt.% oxygen in the processed material.

3. Limitations and Scope for Further Research

The major limitations and scope for further research are identified and listed below based on the literature reviewed in the area of Additive manufacturing of α-β Ti alloy components through SLM and LMD processes.

   i. Limited investigations have been reported with the build geometry [8, 90] which is a major deciding factor to understand the solidification pattern. Hence, it is essential to extend the build geometry research. Vertical built up and horizontal laying may be used to build Ti-6Al-4V specimens using SLM technology and further research with respect to macrostructure, microstructure, texture orientation, mechanical properties such as fatigue strength, tensile strength, creep strength and micro-hardness.

ii. Post heat treatment studies reveal that there exists challenge in achieving the appropriate microstructure, mechanical soundness (specifically the ductility) [34, 35] and good surface finish. The underlying mechanism to withstand cyclic loads and to achieve the required fatigue strength and creep resistance is not well documented. Heat treatment studies on the built specimens may be carried out at 1050°C, 800°C and 650°C. Varying cooling rate in the order of 50°C/h, 250°C/h, 500°C/h and higher quench rates may produce the optimum parameters for desired microstructure and mechanical properties.

iii. There is a paucity of comparative studies on the subsequent influence of varying alloying elements in the metal powder for additive manufacturing [54, 55, 84]. Other than α and β stabilizing elements, the role of neutral elements also needs to be investigated further. Laser deposition of Ti-6Al-2Sn-2Mo-2Cr-0.25Si metal powder on Ti substrate may be experimented which is not reported in the literature.

iv. Investigation of bulk crystallographic texture and micro texture in the as-formed and in heat treated condition has not been carried out comprehensively using techniques such as orientation imaging microscopy (OIM) and electron backscattered diffraction (EBSD). These studies will reveal the grain boundary angle and grain size distribution which is an essential input for improving the micro hardness [39-42, 64].

v. Metallographic and texture (micro and bulk) orientation studies can be made on the laser deposited Ti-6Al-2Sn-2Mo-2Cr-0.25Si at different zones like clad, fusion zone, heat affected zone and in the substrate. The phenomena like local property effects, orientation variations within individual grains, grain size distribution and phase relationships may be studied.

vi. In multi bead deposition of Ti composites, the hardness vary from top to bottom layers which is due to the difference in impurity level [74, 75]. In addition, the layer bonding varies with multi-bead deposition. This can be compensated by varying the process parameters while depositing beads from bottom to top. Need exist for the optimization of process parameters including laser power, scanning speed, powder flow rate and gas flow rate to achieve proper layer bonding without porosity and uniform hardness throughout the layers in Ti-6Al-2Sn-2Mo-2Cr-0.25Si deposition.

vii. Significant work has not been carried out to study the creep behaviour of SLM and LMD made components. For aircraft applications, a comprehensive knowledge about these behaviour is highly essential and worth carrying research.

viii. Remote additive manufacturing is not documented in the review of literature. This technique would be highly essential in the repair of worn-out or damaged components for defence applications in the war front.

ix. Real time identification of defects, stress, microstructure and composition during manufacturing process is unexplored. In-situ identification of phase transformation would save enormous amount of capital resource of materials and human time usually spent in reactive responses.

x. Reliability studies carried out in multi-layer deposited components are not adequately reported. Conventional statistical quality control will not suit AM

and hence in-process control is very much necessary. Certification standards have to be developed for additive manufacturing

4. Conclusions

In this review, an overview of the micro/macrostructures as well as resulting mechanical properties of SLM and LMD processed α-β Ti alloy and CP-Ti component has been presented. Also the effects of processing parameters are discussed.

Predominantly it is reported that during solidification of α-β Ti alloy, columnar prior β-grains grow epitaxially across several layers and against the heat flow. However, most of the work has been made under laboratory conditions without achieving repeatability in the structure and properties. Surface finish and ductility are still lacking behind wrought or conventionally formed material of same alloy. These are due to process factors such as laser intensity, powder flow /wire feed rate, metal deposition strategy, etc., which still needs to be optimized for the specific application, size and shape of components. This is a major hurdle in employing mass production to additive manufacturing, particularly for parts used in high risk fields like aerospace, nuclear and bio-medical.

Reduction of support structures have been carried out using hybrid manufacturing process and multi-axis deposition. Wire feed control in multi bead deposition and predictions of thermal history have been analyzed separately by developing few algorithms. However, these are found to have certain limitations in the integration of build geometry, multi bead deposition and solidification pattern.

The limitations and future research requirements of additive manufacturing α-β Ti alloy components through SLM and LMD are recognized and suggestions to overcome the problems are also discussed.

Wide spectrums of investigations are reviewed in this article on the topic of additive manufacturing α-β Ti alloy components through SLM and LMD. Based on the discussions made here, it is clearly understood that, well optimized process parameters supported by modelling and simulation would make SLM and LMD processed CP-Ti and α-β Ti alloy composites viable choices for commercial applications. The information provided in this article is intended to equip the researchers working in this field with an overview of some methods of additive manufacturing and the metallurgy of the Ti-6Al-4V alloy and its variants.

References

1. Gary, K.L.; and Eric, S. (2000). Practical considerations and capabilities for laser assisted direct metal deposition. *Materials & Design*, 21, 417-423.
2. Abe, F.; Osakada, K.; Shiomi, M.; Uematsu, K.; and Matsumoto, M. (2001). The manufacturing of hard tools from metallic powders by Selective Laser Melting. *Journal of Materials Processing Technology*, 111, 210-213.
3. Griffith, M.L.; Schlienger, M.E.; Harwell, L.D.; Oliver, M.S.; Baldwin, M.D.; and Ensz, M.T. (1999). Understanding thermal behavior in the LENS process. *Materials & Design*, 20, 107-113.

4. Das, S. (2003). Physical aspects of process control in selective laser sintering of metals. *Advanced Engineering Materials*, 5, 701-711.

5. Kumar, S. (2003) Selective laser sintering: A qualitative and objective approach. *Journal of the Minerals*, *Metals & Materials Society* 2003, 55, 43-47.

6. Kruth, J.P.; Levy, G.; Klocke, F.; and Childs, T.H.C. (2007). Consolidation phenomena in laser and powder-bed based layered manufacturing, *CIRP Annals-Manufacturing Technology*, 56, 730-759.

7. Gu, D.; and Shen, Y. (2009). Balling phenomena in direct laser sintering of stainless steel powder: Metallurgical mechanisms and control methods, *Materials & Design*, 30, 2903-2910.

8. Paydas. H.; Mertens, A.; Carrus, R.; Lecomte-Beckers, J.; and Tchoufang, T.J. (2015). Laser cladding as repair technology for Ti-6al-4v alloy: Influence of building strategy on microstructure and hardness. *Materials & Design*, 85, 497-510.

9. Bernd, B.; Erhard, B.; and Omer, B. (2011). Wire based additive layer manufacturing: Comparison of microstructure and mechanical properties of TI-6AL-4V components fabricated by laser-beam deposition and shaped metal deposition. *Journal of Materials Processing Technology*, 211, 1146-1158.

10. Leong, K.F.; Liu, A.; and Chua, C.K. (2009). *A Practical Approach on Temperature Variation in Selective Laser Melting with a Novel Heat Transfer Model*, In: Innovative Developments in design and manufacturing - Advanced research in virtual and rapid prototyping. The Netherlands: CRC Press, 363-367.

11. Averyanova, M.; Bertrand, P.H.; and Verquin, B. (2012). Studying the influence of initial powder characteristics on the properties of final parts manufactured by the Selective Laser Melting technology. *Virtual and Physical Prototyping*, 6, 215-223.

12. Leu, M.C.; Pattnaik, S.; and Hilmas, G.E. (2012). Investigation of laser sintering for freeform fabrication of zirconium diboride parts. *Virtual and Physical Prototyping*, 7, 25-36.

13. Nikolay, K.T.; Yurii, V.K; Sergei, E.M.; Michail, B.I.; Tahar, L.; and Victor, I.T. (2000). Absorptance of powder materials suitable for laser sintering. *Rapid Prototyping*, 6, 155-161.

14. Glardona, R.; Karapatisa, N.; Romanob, V.; and Levyc, G.N. (2001). Influence of Nd: YAG parameters on the selective laser sintering of metallic powders. *CIRP Annals-Manufacturing Technology*, 50, 133-136.

15. Savalani, M.M.; Hao, L.; and Harris, R.A. (2006). Evaluation of CO2 and Nd:YAG lasers for the Selective Laser Sintering of HAPEX®. Proceedings of the Institution of Mechanical Engineers. Part B: *Journal of Engineering Manufacture*, 220, 171-182.

16. Sanjay, K.; and SisaPityana. (2011). Laser-based additive manufacturing of metals. *Advanced Materials Research*, 227, 92-95.

17. Froes, F.H.; and Dutta, B. (2014). The Additive Manufacturing (AM) of titanium alloys. *Advanced Materials Research*, 1019, 19-25.

18. Vojislav, P.; Juan, V.H.G.; Olga, J.F.; Javier, D.G.; Jose, R.B.P.; and Luis, P.G. (2011). Additive layered manufacturing: Sectors of industrial

application shown through case studies. *International Journal of Production Research*, 49, 1061-1079.

19. Wai, Y.Y.; and Chee, K.C. (2013). A quality management framework for implementing additive manufacturing of medical devices. *Virtual and Physical Prototyping*, 8, 193-199.

20. John, M.M. (2013). Additive manufacturing and its implications for military ethics, *Journal of Military Ethics*, 12, 225-234.

21. Nima, S.; Aref, Y.; Linkan, B.; Scott, M.T. (2015). An overview of direct laser deposition for additive manufacturing; Part II: Mechanical behavior, process parameter optimization and control. *Additive Manufacturing*, 8, 12-35.

22. Mohammad, V.; Srisit, C.; Brian, M.; and Shoufeng, Y. (2013). Multiple material additive manufacturing- Part 1: A review. *Virtual and Physical Prototyping*, 8, 19-50.

23. Wei, G.; Yunbo, Z.; Devarajan, R.; Karthik, R.; Yong, C.; Christopher, B.W; Charlie, C.L.W.; Yung, C.S.; Song, Z.; and Pablo, D.Z. (2015). The status, challenges, and future of additive manufacturing in Engineering. *Computer Aided Design*, 69, 65-89.

24. William, E.F. (2014). Metal additive manufacturing: A review. *Journal of Materials Engineering and Performance*, 23, 1917-1928.

25. Herderick, E. (2011). Additive manufacturing of metals: A review. *Proceedings of MS&T 11. Additive Manufacturing of Metals*, Columbus, OH.

26. Chandramohan, P. (2017). Laser additive manufactured Ti-6Al-4V alloy: Tribology and corrosion studies. *International Journal of Advanced manufacturing Technology*, 92, 3051-3061.

27. Lore, T.; Frederik, V.; Tom, C.; Jan, V.H.; and Jean-Pierre, K. (2010). A Study of the microstructural evolution during Selective Laser Melting of Ti-6Al-4V. *Acta Materialia*, 58, 3303-3312.

28. Beth, E.C.; Todd, A.P.; Allison, M.B. (2015). Anisotropic tensile behaviour of Ti-6Al-4V components fabricated with directed energy deposition additive manufacturing. *Acta Materialia*, 87, 309-320.

29. Abdalla, R.N.; Jayme, S.K.; Edward, W.R.; and Todd, J.S. (2015). Intra-Layer closed-loop control of build plan during directed energy Additive Manufacturing of Ti-6Al-4V. *Additive Manufacturing*, 6, 39-52.

30. Wei-Chin, H.; Chuan-Sheng, C.; Ching-Chih, L.; Chih-Hsien, W.; De-Yau, L.; Sung-Ho, L.; Wen-Peng, T.; and Ji-Bin, H. (2014). Microstructure-controllable laser additive manufacturing process formetal products. *Physics Procedia*, 56, 58- 63.

31. Xu, W.; Brandt, M.; Sun, S.; Elambasseril, J.; Liu, Q.; Latham, K.; Xiad, K.; and Qiana, M. (2015). Additive Manufacturing of strong and ductile TI-6AL-4V by Selective Laser Melting via in situ martensite decomposition. *Acta Materialia*, 85, 74-84.

32. Russell, A.M.; and Lee, K.L. (2005). *Intermetallic compounds, structure-property relations in nonferrous metals.* John Wiley & Sons, Inc., Hoboken, NJ, USA, 474-487.

33. Yadroitsev, I.; Krakhmalev, P.; Yadroitsava, I. (2014). Selective Laser Melting of Ti6Al4V Alloy for Biomedical Applications: Temperature Monitoring and Microstructural Evolution. *Journal of Alloys and Compounds*, 583, 404-409.

34. Erhard, B.; Achim, S.; and Christoph, L. (2015). Morphology, microstructure, and hardness of Titanium (Ti-6Al-4V) blocks deposited by wire-feed Additive Layer Manufacturing (ALM). *Journal of the Mechanical Behavior of Biomedical Materials*, 51, 61-73.

35. Erhard, B.; Frank, P.; Vesselin, M.; Bernd, V.; and Christoph, L. (2011). Mechanical properties of additive manufactured titanium (Ti-6Al-4V) blocks deposited by a solid-state laser and wire. *Materials & Design*, 32, 4665-4675.

36. Erhard, B.; Daniel, G. (2012). Microstructure of Additive Layer Manufactured Ti-6Al-4V after exceptional post heat treatments. *Materials Letters*, 81, 84-87.

37. Wu, S.Q.; Lu, Y.J.; Gan, Y.L.; Huang, T.T.; Zhao, C.Q.; Lin, J.J.; Guo, S.; Lin, J.X. (2016). Microstructural evolution and microhardness of a selective-laser melted Ti-6Al-4V alloy after post heat treatments. *Journal of Alloys and Compounds*, 672, 643-652.

38. Chunze, Y.; Liang, H.; Ahmed Hussein.; Philippe, Y. (2015). Ti-6Al-4V triply periodic minimal surface structures for bone implants fabricated via selective laser melting. *Mechanical Behavior of Biomedical Materials*, 51, 61-73.

39. Vrancken, B.; Thijs, L.; Kruth, J.P.; and Van Humbeeck, J. (2014). Microstructure and mechanical properties of a novel β titanium metallic composite by selective laser melting. *Acta Materialia*, 68, 150-158.

40. RenuKumari.; Tim, S.; Wilhelm, P.; Heino, B.; Jyotsna, D.M. (2015). Laser surface textured titanium alloy (Ti-6Al-4V) - Part II - Studies on bio-compatibility. *Applied Surface Science*, 357, 750-758.

41. Wilhelm. P.; RenuKumari.; Heino, B.; Tim, S.; Jyotsna, (2015). D.M. Laser surface textured titanium alloy (Ti-6Al-4V): Part 1 - surface characterization. *Applied Surface Science*, 355, 104-111.

42. Tiferet, E.; Rivin, O.; Ganor, M.; Ettedgui, H.; Ozeri, O.; Caspi, E.N.; Yeheskel, O. (2016). Structural investigation of selective laser melting and electron beam melting of Ti-6Al-4V using neutron diffraction. *Additive Manufacturing*, 10, 43-46.

43. Alcisto, J.; Enriquez, A.; Garcia, H.; Hinkson, S.; Steelman, T.; Silverman, E.; Valdovino, P.; Gigerenzer, H.; Foyos, J.; Ogren, J.; Dorey, J.; Karg, K.; McDonald, T.; and Es-Said, O.S. (2001). Tensile properties and microstructures of laser-formed Ti-6Al-4V. *Journal of Materials Engineering and Performance*, 20, 203-212.

44. Manikandakumar, S.; Ashwin, P.; Guy, L. (2015). Microstructure and mechanical properties of wrought and additive manufactured Ti-6Al-4V cylindrical bars. *Procedia Technology*, 20, 231-236.

45. Myriam, G.; Patrice, P.; Cyril, G.; Muriel, C.; Simon, M.; Philippe, L.M.; Denis, C.; and Remy, F. (2014). Influence of a pulsed laser regime on surface finish induced by the direct metal deposition process on a Ti64 Alloy. *Journal of Materials Processing Technology*, 214, 485- 495.

46. Jayasheelan, V.; Ruth, D. G.; Richard, J.M.H.; Steven, D.R.C.; Steve, E. (2016). The effect of laser remelting on the surface chemistry of Ti6al4V components fabricated by selective laser melting. *Journal of Materials Processing Technology*, 232, 1-8.

47. Sugahara, T.; Reis, D.A.P.; MouraNeto, C.; Barboza, M.J.R.; Perez, E.A.C; PiorinoNeto, F.; Hirschmann, A.C.O. (2010). The Effect of Widmanstätten and equiaxed microstructures of Ti-6Al-4V on the oxidation rate and creep behavior. *Material Science Forum*, 636-637, 657-662.

48. Haijun, G.; Khalid, R.; Hengfeng, G.; Janaki, R.G.D.; Thomas, S.; Brent, S. (2015). Influence of defects on mechanical properties of Ti-6Al-4 V components produced by selective laser melting and electron beam melting. *Materials & Design*, 86, 545-554.

49. Hualiang, W.; Qizhi, W.; Chenxue, J.; and Zheng, Z. (2016). Multi-scale damage mechanics method for fatigue life prediction of additive manufacture structures of Ti-6Al-4V. *Materials Science & EngineeringA*, 669, 269-278.

50. Rafi, H.K; Karthik, N.V; Haijun, G.; Thomas, L,S.; Brent, E.S. (2013). Microstructures and mechanical properties of Ti6Al4V parts fabricated by selective laser melting and electron beam melting. *Journal of Materials Engineering and Performance*, 22, 3872-3883.

51. Haize G.; Diana, A.L.; Ryan R.D.; Michael M.K.; Peeyush N. (2016). Effects of the microstructure and porosity on properties of Ti-6Al-4V ELI alloy fabricated by electron beam melting (EBM). *Additive Manufacturing*, 10, 47-57.

52. Haijun, G.; Khalid, R.; Hengfeng, G.; Thomas, S.; and Brent, S. (2014). Analysis of defect generation in Ti-6Al-4V parts made using powder bed fusion additive manufacturing processes. *Additive Manufacturing*, 1-4, 87-98.

53. Peng-Hui, L.; Wei-Guo, G.; Wei-Dong, H.; Yu Su.; Xin, L.; Kang-Bo,Y. (2015). Thermomechanical response of 3Dlaser-depositedTi-6Al-4V alloy over a wide range of strain rates and temperatures. *Materials Science & Engineering A*, 647, 34-42

54. Yanyan, Z.; Xiangjun, T.; Jia, L.; Huaming, W. (2015). The anisotropy of laser melting deposition additive manufacturingTi-6.5Al-3.5Mo-1.5Zr-0.3Si Titanium alloy. *Materials & Design*, 67, 538-542.

55. Hai-shui, R.; Xiang-jun, T.; Dong, L.; Jian L.; Hua-ming, W. (2015). Microstructural evolution and mechanical properties of Laser Melting Deposited Ti−6.5Al−3.5Mo−1.5Zr−0.3Si Titanium alloy. *Transactions of Nonferrous Metals Society of China*, 25, 1856−1864.

56. Yanyan, Z.; Xiangjun, T.; Jia, L.; and Huaming, W. (2014). Microstructure evolution and layer bands of laser melting deposition Ti-6.5Al-3.5Mo-1.5Zr-0.3Si titanium alloy. *Journal of Alloys and Compounds*, 16, 468-474.

57. Yao-Jian, L.; Hua-Ming, W. (2015). Influence of prior-β-grain size on tensile strength of a laser-deposited α/β titanium alloy at room and elevated temperatures. *Materials Science & Engineering A*, 622, 16-20.

58. Wang, T.; Zhu, Y.; Zhang, S.; Tang, H.; Wang, H. (2015). Grain morphology evolution behavior of titanium alloy components during Laser Melting Deposition Additive Manufacturing. *Journal of Alloys and Compounds*, 632, 505-513.

59. Ting-ting, Q.; Dong, L.; Xiang-jun, T.; Chang-meng, L.; Hua-ming, W. (2014). Microstructure of TA2/TA15 graded structural material by Laser Additive Manufacturing process. *Transactions of Nonferrous Metals Society of China,* 24, 2729−2736.

60. Yao-Jian, L.; Xiang-Jun, T.; Yan-Yan Z.; Jing, L.; Hua-Ming, W. (2014). Compositional variation and micro structural evolution in laser additive manufactured Ti/Ti-6Al-2Zr-1Mo-1V graded structural material, *Materials Science and Engineering: A*, 599, 242-246.

61. Liu, C.; Wang, H.; Tian, X.; Tang, H.; Liu, D. (2013). Microstructure and tensile properties of Laser Melting Deposited Ti-5Al-5Mo-5V-1Cr-1Fe near β Titanium alloy. *Materials Science and Engineering: A*, 586, 323-329.

62. Liu, C.; Wang, H,; Tian, X.; Liu, D. (2014). Obtaining bimodal microstructure in Laser Melting Deposited Ti-5Al-5Mo-5V-1Cr-1Fe near β Titanium alloy. *Materials Science and Engineering: A*, 609, 77-184.

63. A-li, Z.; Dong, L.; Hai-bo, T.; Hua-ming, W. (2013). Microstructure evolution of laser deposited Ti60A titanium alloy during cyclic thermal exposure, *Transactions of Nonferrous Metals Society of China*, 23, 3249-3256.

64. Qiang, Z.; Jing, C.; Pengfei, G.; Hua, T.; and Xin, L. (2015). Texture and microstructure characterization in laser additive manufactured Ti-6Al-2Zr-2Sn-3Mo-1.5Cr-2Nb titanium alloy. *Materials & Design*, 88, 550-557.

65. Zhuo, L.; Jing, L.;, Jian, L.; Dong, L.; Huaming, W. (2016). Structure and formation mechanism of a/a interface in laser melting deposited α + β titanium alloy. *Journal of Alloys and Compounds*, 657, 278-285.

66. Yao-Jian, L.; Dong, L.; Hua-Ming, W. (2014). Microstructure and mechanical behaviour of commercial purity Ti/Ti-6Al-2Zr-1Mo-1V structurally graded material fabricated by laser additive manufacturing. *Scripta Materialia*, 74, 80-83.

67. Tian, X.; Zhang, S.; Li, A.; Wan, H. (2010). Effect of annealing temperature on the notch impact toughness of a laser melting deposited titanium alloy Ti-4Al-1.5Mn. *Materials Science and Engineering: A*, 527, 1821-1827.

68. Attar, H.; Lober, L.; Funk, A.; Calin, M.; Zhang, L.; Prashanth, K.S.S.; Zhang, Y.; Eckert, J. (2015). Mechanical behaviour of porous commercially pure Ti and Ti-TiB composite materials manufactured by selective laser melting. *Materials Science and Engineering: A,* 625, 350-356.

69. Chunlei, Q.; Ravi, G.; Chris, D.; Andrew, R.; Steve, D.; Moataz, M. (2015). Fabrication of large Ti-6Al-4V structures by direct laser deposition. *Journal of Alloys and Compounds*, 629, 351-361.

70. Eckart, U.; Robert, K.; Tiago, B.; Marcio, F.; Anderson, V. (2015). Additive manufacturing of Titanium alloy for aircraft components. *Procedia CIRP*, 35, 55-60.

71. Parry, L.; Ashcroft, I.A.; Wildman, R.D. (2016). Understanding the effect of laser scan strategy on residual stress in selective laser melting through thermo-mechanical simulation. *Additive Manufacturing*, 12, 1-15.

72. Rasheedat, M.; Esther, T.; Mukul, S.; and Sisa, P. (2013). Laser metal deposition of Ti6Al4V: A study on the effect of laser power on microstructure

and micro-hardness. *In Proceedings of the International MultiConference of Engineers and Computer Scientists* (*IMECS*), Hong Kong.

73. Rasheedat, M.; Esther, T.; and Stephen, A. (2015). Laser power and scanning speed influence on the mechanical property of laser metal deposited titanium-alloy. *Lasers in Manufacturing and Materials Processing*, 2, 43-55.

74. Erhard, B.; Vesselin, M.; Bernd, V.; Christoph, L. (2011). Deposition of Ti-6Al-4V using laser and wire, part II: hardness and dimensions of single beads, *Surface and Coatings Technology*; 206: 1130-1141.

75. Erhard, B.; Vesselin, M.; Bernd, V.; Christoph, L. (2011). Deposition of Ti-6Al-4V using laser and wire, part I: microstructural properties of single beads. *Surface and Coatings Technology*; 206, 1120-1129.

76. Tarak, A.; Joseph, W.; and Frank, L. (2011). Methodology for studying effect of cooling rate during laser deposition on microstructure. *Journal of Materials Engineering and Performance* , 24, 3129-3136.

77. Bartolomeu, F. Faria, S. Carvalho, O. Pinto, E. Alves, N. Silva , F.S. Miranda, G. (2016). Predictive models for physical and mechanical properties of Ti6Al4V produced by Selective Laser Melting. *Materials Science & Engineering A*, 663, 181-192.

78. Rasheedat, M.; Esther, T.; Mukul, S.; and Sisa, P. (2014). Characterization of laser deposited Ti6Al4V/TiC composite powders on a Ti6Al4V substrate. *Lasers in Engineering*; 29: 197-213.

79. Rasheedat M.; Esther, T.; Mukul, S, and Sisa, P. (2013). Scanning velocity influence on microstructure, micro-hardness and wear resistance performance of laser deposited Ti6Al4V/TiC composite. *Materials & Design*, 50, 656-666.

80. Rasheedat, M.; and Esther, T. (2015). Effect of laser power and powder flow rate on the wear resistance behaviour of laser metal deposited TiC/Ti6Al4V Composites. *Materials Today: Proceedings*, 2, 2679 - 2686.

81. Mahamood, R.; Akinlabi, E. (2015). Laser metal deposition of functionally graded Ti6Al4V/TiC. *Materials & Design*, 84, 402-410.

82. Wang, F.; Mei, J.; Jiang, H.; Wu, X. (2007). Laser fabrication of Ti6Al4V/TiC composites using simultaneous powder and wire feed. *Materials Science and Engineering: A*, 445-446, 461-466.

83. Farayibi, P.; Folkes, J.; and Clare, A. (2013). Laser deposition of Ti-6Al-4V wire with WC powder for functionally graded components. *Materials and Manufacturing Processes*, 28, 514-518.

84. Jyotsna, D.M. (2011). Laser gas alloying of Ti-6Al-4V. *Physics Procedia*, 12, 472-477.

85. Monnamme, T.; Esther, A.; Mukul, S.; Sisa, P. (2014). Microstructures, hardness and bioactivity of hydroxyapatite coatings deposited by direct laser melting process. *Materials Science and Engineering: A*, 43, 189-198.

86. Attar, H.; Calin, M.; Zhang, L.; Scudino, S.; and Eckert , J. (2014). Manufacture by selective laser melting and mechanical behavior of commercially pure titanium*, Materials Science and Engineering: A* 2014, 593, 170-177.

87. Dongdong, G.; Yves-Christian, H.; Wilhelm, M.; Guangbin, M.; Rui, J.; Konrad, W.; Reinhart, P. (2012). Densification behaviour, microstructure evolution, and wear performance of selective laser melting processed commercially pure titanium. *Acta Materialia*, 60, 3849-3860.

88. Yali, L.; and Dongdong, G. (2014). Thermal behaviour during selective laser melting of commercially puretitanium powder: Numerical simulation and experimental study. *Additive Manufacturing*, 1-4, 99-109.

89. Hooyar, A.; Matthias, B.; Mariana, C.; Lai-Chang, Z.; Sergio, S.; and Jurgen, E. (2014). Selective laser melting of in situ titanium-titanium boride composites: Processing, microstructure and mechanical properties. *Acta Materialia*, 76, 13-22.

90. Chunlei, Q.; Ravi, G.A; Moataz, M.A. (2015). Microstructural control during direct laser deposition of β-titanium alloy. *Materials & Design*, 81, 21-30.

91. Zhang, C.; Klemm, D.; Eckert, J.; Haod, Y.; and Sercombea, T. (2011). Manufacture by SLM and mechanical behaviour of biomedical Ti-24Nb-4Zr-8Sn alloy. *Scripta Materialia*, 65, 21-24.